SENSITIVITY STUDY OF COMB-DRIVE ACTUATOR WITH FOLDED SUSPENSION

V. KRYLOV[1], N. MOUSSAY[2] AND Y. BERNSTEIN[2]
[1] Department of Solid Mechanics Materials and Systems, Tel Aviv University, Israel
[2] Teraop Ltd., Israel

ABSTRACT

Comb-drive electrostatic actuators are widely used in micron scale devices. The main failure mechanisms of this kind of actuator include electrostatic instability as well as the inability to meet performance requirements imposed by their particular applications. In the present work, the sensitivity of the comb-drive actuators of different configurations to the actuator geometry and ambient temperature are studied both theoretically and experimentally. Displacement-voltage dependence, stability range and natural frequencies are used as output parameters. Models of the actuator include definitions based on an extensible elastica theory as well as reduced order models. The influence of secondary compliances of the structure is studied using the Finite Element Method. Results produced by the models, and proven experimentally, show that the location of the instability point is sensitive to geometric imperfections and secondary compliances while the influence of temperature is relatively minor. Highly uncertain fabrication tolerances may lead to a significant reduction in the stiffness of the device. Stiffness parameters are extracted by fitting the static and dynamic responses as well as direct measurements of the device geometry.

1 INTRODUCTION

The lateral comb-drive actuator is one of the most widely used components of MEMS based devices. Comb drive actuators were first integrated in polysilicon resonators (Tang *et al* [1]). Progress in the Deep Reactive Ion Etching (DRIE) technique resulted in the development of large displacement comb drive actuators for optical applications such that Variable Optical Attenuators (VOA, e.g., Lee [2]) and optical switches, where movable parts serve as optical elements as well. In these applications, the actuator should provide repeatable operation and low sensitivity to operational conditions, mainly ambient temperature and mechanical vibrations. In addition, stability range should be maximized while actuation voltage and actuator dimensions are kept as small as possible. Comb drive actuators are used also as loading devices for micron scale material testing (e.g., see Haque *et al* [3]).

It should be noted that actuators fabricated using DRIE are characterized by high aspect ratio (typically ten to one and higher) between vertical and lateral dimensions and, consequently, between out of plane and in plane compliances. As a result, large actuator displacement is possible. Displacements are usually limited by electrostatic instability, commonly referred to as side pull-in (Legtenberg *et al* [4]). On the other hand, uncertainty in device parameters originating in the fabrication process may affect the structural integrity of the actuator and device performance. For example, the footing effect, an over etch of material that occurs at the base of the etched structures, has a strong influence on the geometry and affects both stiffness of the structural elements and actuating force (e.g., see Lee *et al* [5]). In the present work, we study, both theoretically and experimentally, the sensitivity of the DRIE fabricated comb-drive actuators of different configurations to the actuator geometry and operation conditions.

2 MODEL

The device under consideration is shown in Fig. 1 and incorporates a movable shutter suspended by flexible beams arranged into one or two folded suspensions. Electrostatic force applied to movable combs is transferred to the shutter through transverse arms.

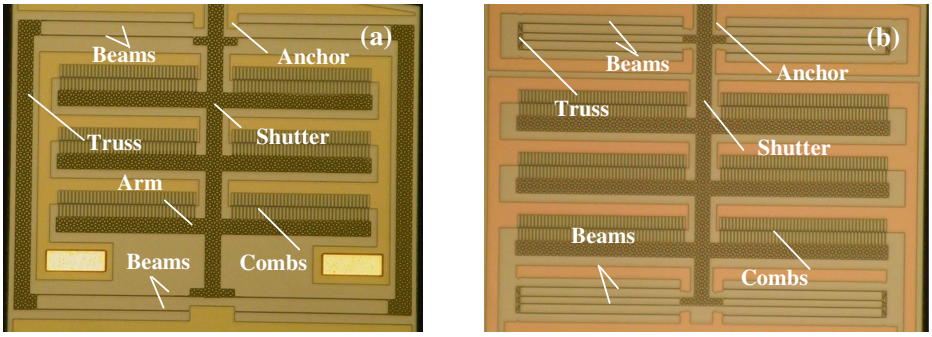

Figure 1: Comb-drive actuators with one (a) and two (b) folded suspensions.

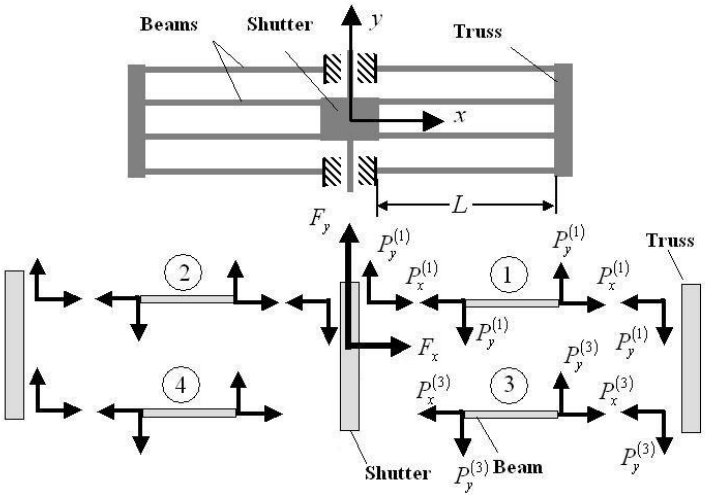

Figure 2: Folded suspension modeled as an assembly of rigid and flexible elements.

Side instability of comb drive actuators was studied by Legtenberg *et al* [4]. The expression for maximal displacement $v_{\max}$ was obtained based on a simplified model of folded suspension assembled of four similar beams

$$v_{\max} = d\sqrt{\frac{k_x}{2k_y}} - \frac{y_0}{2}, \qquad k_y = \frac{24EI}{L^3}, \qquad k_x^0 = \frac{2EA}{L}, \qquad k_x^y = \frac{200EI}{3Lv^2}, \qquad \frac{1}{k_x} = \frac{1}{k_x^0} + \frac{1}{k_x^y}. \tag{1}$$

Here k_x and k_y are stiffness in the lateral and axial directions, respectively (Fig. 2), E is the Young's modulus, L is suspension length, I and A are moment of inertia and area of the beam's cross-section, d is electrostatic gap between combs and y_0 is initial overlap between combs. This model was used by several researchers for the prediction of stable travel of comb actuators (e.g., Grade *et al* [6]). We present below a refined model based on the extensible elastica description of the suspension. The model serves as a reference solution and permits the study of the influence of geometric nonlinearity and axial forces acting along the beams on the response.

2.1 Extensible elastica model of folded suspension

The actuator is modeled as an assembly of a rigid shutter and truss and flexible beams, Fig. 2. It is also assumed that rotational motion of the truss and of the shutter around z axis is precluded.

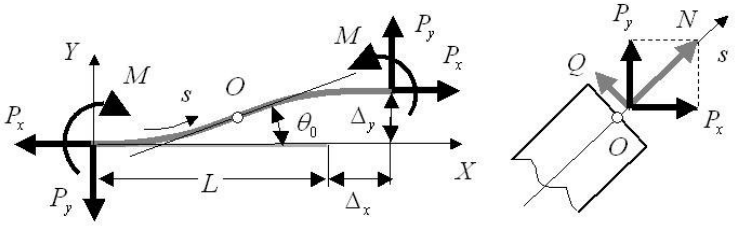

Figure 3: Notations for a beam large deformation analysis.

Equilibrium and compatibility equations of the assembly have the form

$$\hat{P}_x^{(2)} - \hat{P}_x^{(1)} = \hat{F}_x, \quad \hat{P}_x^{(3)} = -\hat{P}_x^{(1)}, \quad \hat{P}_x^{(4)} = -\hat{P}_x^{(2)}, \quad \hat{P}_y^{(2)} - \hat{P}_y^{(1)} = \hat{F}_y, \quad \hat{P}_y^{(3)} = -\hat{P}_y^{(1)}, \quad \hat{P}_y^{(4)} = -\hat{P}_y^{(2)}, \tag{2}$$

$$\hat{\Delta}_x^{(3)} + \hat{\Delta}_x^{(4)} = \hat{\Delta}_x^{(1)} + \hat{\Delta}_x^{(2)}, \qquad \hat{\Delta}_y^{(3)} + \hat{\Delta}_y^{(4)} = \hat{\Delta}_y^{(1)} + \hat{\Delta}_y^{(2)}. \tag{3}$$

Here $\hat{\Delta}_x^{(i)} = \Delta_x^{(i)} / L$ and $\hat{\Delta}_y^{(i)} = \Delta_y^{(i)} / L, \quad i = 1..4$ are non-dimensional relative deflections between the ends of the i^{th} beam in positive x and y directions respectively. Non-dimensional electrostatic forces $\hat{F}_x = F_x / N_e$ and $\hat{F}_y = F_y / N_e$ are normalized by the Euler force $N_e = \pi^2 EI / L^2$ and are calculated using the expressions

$$\hat{F}_x = \frac{\beta}{4} \frac{\hat{y}_0 + \hat{v}_0}{(1 - \hat{u}_0 - \hat{\delta})^2} - \frac{\beta}{4} \frac{\hat{y}_0 + \hat{v}_0}{(1 + \hat{u}_0 + \hat{\delta})^2}, \qquad \hat{F}_y = \frac{\beta}{4} \frac{1}{1 - \hat{u}_0 - \hat{\delta}} + \frac{\beta}{4} \frac{1}{1 + \hat{u}_0 + \hat{\delta}}, \tag{4}$$

where $\beta = \varepsilon_0 nhV^2 / (N_e d)$ is voltage parameter, ε_0 is permittivity of free space, n is number of combs, h is the thickness of the device, $\hat{u}_0 = [\hat{\Delta}_x^{(3)} - \hat{\Delta}_x^{(1)}](L/d)$ and $\hat{v}_0 = [\hat{\Delta}_y^{(3)} - \hat{\Delta}_y^{(1)}](L/d)$ are non-dimensional displacements of the shutter in x and y directions respectively and $\hat{\delta} = \delta / d$ is imperfection of the electrostatic gap. The dependence $\hat{\Delta}_x^{(i)} = \hat{\Delta}_x^{(i)}(\hat{P}_x^{(i)}, \hat{P}_y^{(i)}), \quad i = 1..4$ is obtained using extensible elastica theory (e.g., see Brivtek [7]).

The beam in Fig. 3 is shown in its deformed position. The axis X coincides with the undeformed central axis while s is the arc length of the deformed axis. The sum of the projections of the forces in s direction $\hat{N} = \hat{P}_x \cos\theta + \hat{P}_y \sin\theta$ combined with the constitutive equation leads to the expression for stretching λ of the central axis in terms of end forces and slope, θ

$$\hat{N} = (\lambda - 1 - \alpha\Delta T) / (\pi^2 \hat{r}^2), \qquad \lambda = \pi^2 \hat{r}^2 (\hat{P}_x \cos\theta + \hat{P}_y \sin\theta) + \alpha\Delta T + 1. \tag{5}$$

Here $\hat{r} = r / L$ is the non-dimensional gyration radius, α is coefficient of thermal expansion and ΔT is temperature increase. In view of Eq. (5), and with kinematic relations $ds / dX = \lambda, \quad 1 + du / dX = \lambda \cos\theta, \quad dv / dX = \lambda \sin\theta$ in mind, it is possible to write the moment equilibrium equation in the form

$$\frac{1}{\pi^2}\frac{d^2\theta}{d\hat{X}^2} = (1+\alpha\Delta T)(\hat{P}_x \sin\theta - \hat{P}_y \cos\theta) + \pi^2 r^2[(\hat{P}_x^2 - \hat{P}_y^2)\cos\theta\sin\theta - \hat{P}_x \hat{P}_y (\cos^2\theta - \sin^2\theta)]. \quad (6)$$

Here $\hat{X} = X/L$. Note that an inextensible case can be obtained by inserting $\hat{r} = 0$ in Eq. (6). Integration of Eq. (6) under the condition of zero bending moment at $\hat{X} = 1/2$ leads to the equation which relates the end forces $\hat{P}_x$ and $\hat{P}_y$ and the slope θ_0 at the central point

$$\int_0^{\theta_0} \left\{(\hat{N}_0 - \hat{N})[1 + \alpha\Delta T + 1/2\pi^2\hat{r}^2(\hat{N}_0 - \hat{N})]\right\}^{-1/2} d\theta = 2^{-1/2}\pi, \quad (7)$$

where $\hat{N}_0$ is the axial force at the middle point of the beam. Finally, relative deflections between the end points of the beam are given by the expressions $\hat{\Delta}_x = \int_0^1 \lambda\cos\theta d\hat{X} - 1$, $\hat{\Delta}_y = \int_0^1 \lambda\sin\theta d\hat{X}$. Equations Eq. (2), (3) and (7) represent the system of 12 nonlinear equations with respect to $\hat{P}_x^{(i)}$, $\hat{P}_y^{(i)}$, $\theta^{(i)}$, $i = 1..4$. This system is solved numerically using the Matlab software package. Despite that the integrals in Eqs. (6), (7) can be reduced to elliptic integrals, special quadrature formulas were used in order to handle weak singularities appearing in these integrals.

2.2 Reduced order model

Potential energy of the deformed beam written in non-dimensional form is given by the expression

$$\hat{\Pi} = \frac{1}{2\pi^2}\int_0^1 \left(\frac{d\theta}{d\hat{X}}\right)^2 d\hat{X} + \frac{1}{2\pi^2\hat{r}^2}\int_0^1 (\lambda - 1)^2 d\hat{X} - \hat{P}_x\hat{\Delta}_x - \hat{P}_y\hat{\Delta}_y, \quad (8)$$

where $\hat{\Pi} = \Pi/(N_e L)$. Representing the slope in the form $\theta = \theta_k\phi_k(\hat{X})$, limiting the expansion by one term approximation $\theta = 4\theta_0\hat{X}(1-\hat{X})$ and implementing the Rayleigh-Ritz procedure, the expressions of θ_0, $\hat{\Delta}_x$ and $\hat{\Delta}_y$ are obtained in terms of end forces $\hat{P}_x$ and $\hat{P}_y$

$$\theta_0 = \frac{5}{4}\frac{\pi^2\hat{P}_y(1+\pi^2\hat{P}_x)}{10 + \pi^2[\hat{P}_x + \pi^2\hat{r}^2(\hat{P}_x^2 - \hat{P}_y^2)]}, \quad (9)$$

$$\hat{\Delta}_x = \alpha\Delta T - \frac{4}{15}(1+\alpha\Delta T)\theta_0^2 + \pi^2\hat{r}^2\left[\hat{P}_x\left(1 - \frac{2}{15}\theta_0^2\right) + \frac{2}{3}\hat{P}_y\theta_0\right],$$

$$\hat{\Delta}_y = \frac{2}{3}(1+\alpha\Delta T)\theta_0 + \pi^2\hat{r}^2\left(\frac{2}{3}\hat{P}_x\theta_0 + \frac{8}{15}\hat{P}_y\theta_0^2\right). \quad (10)$$

In the derivation of Eqs. (9), (10), it is assumed $\theta_0 << 1$ and that all trigonometric functions are expanded into Taylor series up to the quadratic order. Using Eqs. (9), (10), the system of eight equations Eqs. (2), (3) is solved numerically with respect to $\hat{P}_x^{(i)}$, $\hat{P}_y^{(i)}$ $i = 1..4$.

2.3 Model results

The influence of imperfections and ambient temperature is studied using the models described above. Calculations show that the influence of imperfections on the lateral motion and the stability range of the actuator is essential (see Fig. 4a). Stability range given by Eq. (1) can be viewed therefore as an upper boundary. On the other hand, it was found that the influence of the ambient temperature on the stability is minor.

In addition, a three-dimensional Finite Element model of the actuator was built using commercial (ANSYS) package. Electrostatic loading is applied using transducer element TRANS126 that couples mechanical and electrical degrees of freedom. It was found that the discrepancy between the results produced by the accurate and FE models is relatively large (1.15% for $\hat{v}_0 \sim 1/20$) due to the influence of compliances of the truss and of the shutter. These compliances are an important factor reducing the stability range of the structure. Stable deflection of the actuator without imperfections obtained using FE model is essentially lower than predicted theoretically (Fig. 4 b).

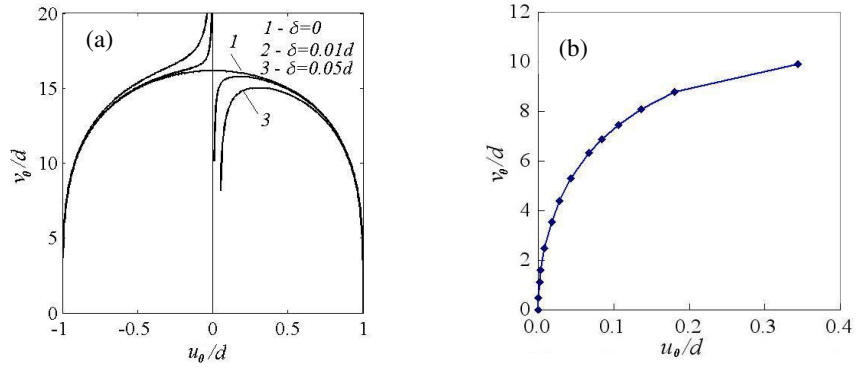

Figure 4: Influence of imperfections (a) and secondary compliances (b) on the equilibrium path. Length to gap ratio is $L/d = 230$.

3 EXPERIMENT

Comb drive actuators of various configurations were fabricated by DRIE using an SOI wafer as starting material. The static response of the actuator was registered by CCD camera and image processing was used for quantitative characterization of the motion. Static and dynamic response of the actuators integrated into a VOA was reconstructed also through the combined use of static voltage-displacement curves obtained by image processing and voltage-attenuation curves obtained through optical power measurements. The natural frequencies are extracted from the spectrum of the response to step function excitations and from resonance curves obtained through the vibration tests. Results of experiments show that significant discrepancies between measured and calculated static and dynamic responses are observed. Direct measurements of the device geometry reveal the reduction in the width of beams and combs originating in the DRIE process. When measured dimensions are used in calculations, good accordance between experimental and theoretical results is observed.

Since the direct measurements of the actuator geometry are destructive and are not always available, a simple parameters extraction procedure was implemented. The compliance $S_i = v_{0i}/V_i^2$ of the i^{th} actuator was extracted by fitting the experimental data. The ratio between the compliances of actuators with differing geometries leads to the system of algebraic equations in terms of geometric parameters (see Eq. (1))

$$\frac{n_i L_i^3}{n_j L_j^3}\frac{(d_j-\delta d)(b_j-\delta b)^3}{(d_i-\delta d)(b_i-\delta b)^3}=\frac{S_i}{S_j}, \qquad S_i=\frac{1}{2}\frac{\varepsilon_0 n_i L_i^3}{E(d_i-\delta d)(b_i-\delta b)^3}. \tag{11}$$

Here δd and δb are over etch of the electrostatic gap and of the width of the beam respectively. Comparison between extracted and measured values reveals satisfactory agreement between the two.

Side pull-in instability was studied as well. Only lateral instability, without rotation of the shutter, was observed. In most cases, the instability at displacements lower that theoretical value was registered (Fig. 5b), especially for actuators with long compliant shutters where much shorter-up to 45% - than predicted theoretically stable displacements were observed. . On the other hand, an increase in the electrostatic gap due to over etch can increase the stable displacement (see Eq. (1)). One can conclude therefore that the prediction of the response and stability range of large displacement DRIE fabricated comb drive actuators requires accounting for the geometric uncertainties, secondary compliances and imperfections. Preliminary characterization of the influence of the fabrication process on the device geometry is essential.

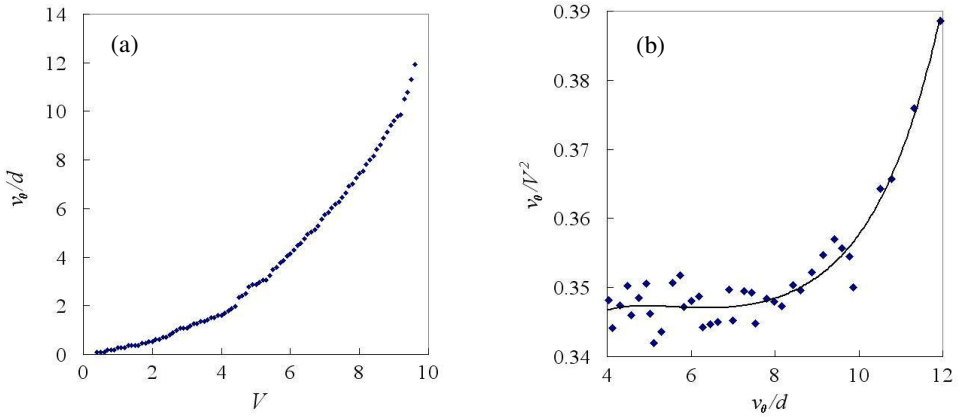

Figure 5: Experimental voltage-displacement curve (a) and compliance fit (b) of the actuator. The increase of the compliance is indicative on the instability. Theoretically predicted stable range is $v_0 / d = 16$.

REFERENCES

[1] Tang, W. C., Nguyen, T-C. H., Judy M. W. and Howe, R. T., "Electrostatic-comb drive of lateral polysilicon resonators," *Sensors and Actuators,* **A21 –A23**, pp. 328 –331, 1990.

[2] Lee, J. H., Kim, Y. Y., Yun, S. S., Kwon, H., Hong, Y. S., Lee, J. H. and Jung S. C., "Design and characteristics of a micromachined variable optical attenuator with a Silicon optical wedge," *Optics Communications,* **221**, pp. 323–330, 2003.

[3] Haque, M. A. and Saif, A., "Microscale materials testing using MEMS actuators," *J. of MEMS*, **10**, pp. 146-152, 2001.

[4] Legtenberg, R., Groenveld, A.W. and Elwenspoek, M., "Comb-drive actuators for large displacements," *J. of MEMS,* **6**, pp. 320-329, 1996.

[5] Lee, J.-Y., Kim, S.-H., Lim, H.-T., Kim, C.-H., Baek, C.-W. and Kim, Y.-K., "Electric spring modeling for a comb actuator deformed by the footing effect in deep reactive ion etching," *J. Micromech. Microeng*. **13**, pp. 72–79, 2003.

[6] Grade, J.D., Jerman, H. and Kenny, T. W., "Design of large deflection electrostatic actuators," *J. of. MEMS,* **12**(3), pp. 335-343, 2003.

[7] Brivtek, S.J., The stability of elastic systems, Pergamon Unified Engineering Series, 1973.

ACKNOWLEDGMENTS. The experimental part of the work was performed at TeraOp. Ltd. The authors would thank O. Avsian, Y. Birman, B. Glushko, A. Gevorkian, K. Hilel, A. Huber, D. Kin, M. Medina and D. Schreiber for their help with this work.